RSC Advances

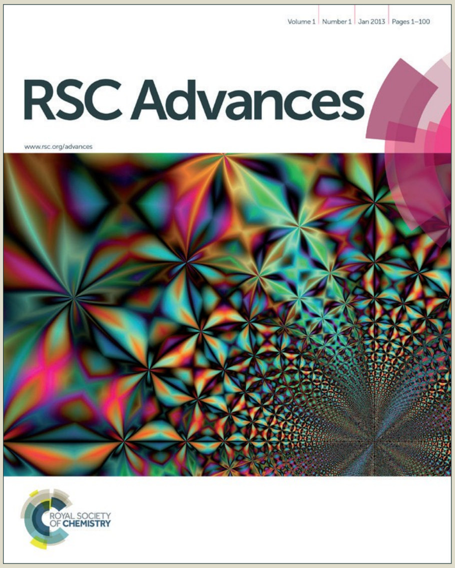

Dynamic Article Links ►

Cite this: DOI: 10.1039/c0xx00000x

www.rsc.org/xxxxxx

ARTICLE TYPE

Glycerol steam reforming over La-Ce-Co mixed oxide-derived cobalt catalysts

M. Surendar, T. V. Sagar, B. Hari Babu, N. Lingaiah, K. S. Rama Rao and P. S. Sai Prasad*

Received (in XXX, XXX) Xth XXXXXXXXX 20XX, Accepted Xth XXXXXXXXX 20XX

DOI: 10.1039/b000000x

La-Ce-Co mixed oxide derived Co catalysts were prepared by co-precipitation method varying the molar ratio of Ce/La in the range of 0.1- 0.9, keeping Co content constant (1 mol). The physico-chemical properties of the samples were investigated by Atomic Absorption Spectrometer(AAS), X-ray diffraction (XRD), Laser Raman spectroscopy, Scanning electron microscopy (SEM), X-ray photoelectron spectroscopy (XPS), UV- diffused reflectance spectroscopy, BET surface area, hydrogen chemisorption and temperature programmed reduction techniques. These catalysts, after reduction, were evaluated for glycerol steam reforming in the temperature range of 500-700 ºC and at atmospheric pressure. The characterization results of catalysts after reduction revealed the collapse perovskite structure and dispersion of Co-metal on the mixed oxide (La_2O_3-CeO_2) support. The possibility for tuning the dispersion of the Co metal for deriving maximum activity and minimum coke formation was examined. The catalyst derived from the mixed oxide, $La_{0.7}Ce_{0.3}CoO_3$, exhibited the best catalytic activity at 700 °C with complete conversion of glycerol and 68% hydrogen yield. Active cobalt area contributes major part of the BET surface area of the reduced catalysts, and this is correlated well with the turn over frequency (TOF). The high dispersion with the formation of Co particles of 4-5 nm size, helped in achieving low coke formation.

1. Introduction

After realizing that global warming is majorly caused by burning of fossil fuels, the search for renewable feedstock has been intensified to meet the energy requirements of the world. Biomass conversion to hydrogen has thus acquired greater prominence. The advantage of using hydrogen in fuel cells has further enhanced its significance in the energy conversion and management sector[1]. Glycerol, which is obtained as a by-product in biodiesel production, can form an important source for hydrogen generation. More and more crude glycerol would be available as the production of biodiesel increases. The direct use of crude glycerol in food, health care and pharmaceutical industry is not possible due to the presence of unreacted methanol, catalyst residues and water as impurities. Since purification is cumbersome and expensive, proper utilization of crude glycerol becomes an important issue for improving the economics of biodiesel production. An efficient application of crude glycerol is to generate hydrogen by steam reforming, thus affording clean energy[2-5] made available to the fuel industry.

Among the different reforming processes for glycerol conversion to hydrogen, aqueous phase reforming (APR)[6–9] and steam reforming (SR)[10–13] are well investigated. APR is a pressure process and offers lower hydrogen selectivity. SR, on the other hand, is favourable even at atmospheric pressure. However, the endothermic nature of SR demands high reaction temperatures leading to the formation of a variety of products and severe coking of catalyst. Thus, the design of catalyst becomes a challenging task.

The reactions associated with steam reforming process are summarized below.

$C_3H_8O_3+3H_2O \rightarrow 7H_2+3CO_2$ — — — Steam reforming

$C_3H_8O_3 \rightarrow 4H_2+ 3CO$ — — — Direct decomposition

$CO + H_2O \rightarrow H_2+ CO_2$ — — — WGS reaction

$CO + 3H_2 \rightarrow CH_4 + H_2O$ — — — Methanation

$CH_4 + CO_2 \rightarrow 2H_2+ 2CO$ — — — Methane dry reforming

$2CO \rightarrow CO_2+C$ — — — Carbon formation

Pd[14], Ir, Co[15], Rh, Ru[14], Pt[14,16] and Ni[14, 15, 17, 18] are investigated as catalysts for the steam reforming reaction. The noble metals are considered economically less viable because of their low availability and high cost. Though, Ni is cheaper compared to the noble metals it is associated with severe

---

Inorganic and Physical Chemistry Division, CSIR-Indian Institute of Chemical Technology, Hyderabad-500 607, India,
Corresponding author; E-mail: saiprasad@iict.res.in

coking under reforming conditions. Extensive work has been reported in the literature to make Ni catalysts more adoptive, especially for the steam reforming of glycerol[19, 20]. Recent review on glycerol steam reforming illustrating the several challenging issues in producing the highly pure hydrogen[21]. The new concept like continuous sorption-enhanced steam reforming by moving-beds and riser systems[19, 21], sorption enhanced chemical looping chemical looping[1] was efficient methods and offering the good stability for the catalysts. Highly dispersed Ni particles are recommended for suppressing the carbon formation to a great extent[22]. The attainment of such small particles depends on factors like the method of preparation, type of precursor used in the preparation[23], calcination and reaction temperatures[24]. Replacement of the conventional catalysts with well defined structures like hydrotalcites, and modification of the support and active metal with suitable promoters[25] are reported. CeO_2 modification of Al_2O_3 is stated to have stabilized the Ni° particles by enhancing nickel-ceria interactions. However, higher ceria content reduces the capacity of the Ni catalyst to convert intermediate oxygenated hydrocarbons into H_2. Ni catalysts with basic oxide supports (Ex. dolomite, MgO) afford a much higher conversion of glycerol and the selectivity towards hydrogen than the acidic oxide supports (Ex. SiO_2, Al_2O_3)[26]. Molybdate modification is found to decrease the acidity and the strong metal-support interaction in Ni/γ-Al_2O_3 catalyst leading to a stable catalytic activity[27]. The substitution of 50% La with Ce in $LaNiO_3$ mixed oxide has provided more deactivation-resistant catalyst, through the CeO_2-La_2O_3 solid solution formation[28]. Synergetic interaction of La and Ca in $La_{0.5}Ca_{0.5}NiO_3$ is found to increase the metal dispersion and minimize coke formation over the Ni sites[29]. The addition of small amount of lanthana (3 wt. %) to Al_2O_3 support is advantageously adopted to improve metal dispersion and decrease Ni particle size[30]. Similarly, the inclusion of CaO to ZrO_2 is shown to enhance the reforming activity of Ni by minimizing the carbon formation[31]. Pt is a good promoter to increase the reducibility of Ni catalysts through the H_2 spillover. The side reactions are prevented, thereby increasing the catalytic activity[32]. Cu insertion into the $LaNiO_3$ perovskite has minimized the sintering of Ni particle offering good stability to the catalyst [33].

Though Co based catalysts are more resistant to carbon deposition than the Ni based ones, detailed work as described above, has not been done in the identification of the influence of particle size on the activity and coke resistance in steam reforming of glycerol. Coke formation in steam reforming can be minimized by fixing the active metal in a well-defined structure like perovskite[34]. These structures enhance the activity and stability[35], because they lead to nanosized particles of active metal well dispersed on the supports[36], during the course of pre-reduction. La and Co containing perovskites have been widely studied for oxidation reactions, with the incorporation of Ce in it. Ce sets up redox couple under the reaction conditions and it also possesses high oxygen storage capacity. These characteristics of the catalyst have been exploited in CO oxidation. In the case of WGS reaction it is used to maximize hydrogen production[37-41]. La_2O_3 on the other hand, imparts stability to the catalyst[42,43]. Co in combination with La and Ce would be advantageous for the maximization of hydrogen selectivity. The aim of this work is to tune Co dispersion in order to arrive at maximum hydrogen yield and minimum coke formation during the reforming reaction. La-Ce-Co mixed oxides, with varying La/Ce ratio, are selected as precursors.

2. Experimental

2.1 Catalyst preparation

The $La_xCe_{1-x}CoO_3$ (x=0.1, 0.3, 0.5, 0.7, 0.9) mixed oxides were prepared by co-precipitation method. Requireed quantities of the nitrate salts of the metals [$La(NO_3)_3{\cdot}6H_2O$, $Ce(NO_3)_3{\cdot}6H_2O$ and $Co(NO_3)_2{\cdot}6H_2O$ (99.0%, Sigma Aldrich)] were dissolved in water and the precipitation was carried out using 5 % aq. NH_4OH with rigorous stirring, maintaining the pH at 10. The resulting precipitate was filtered, washed with distilled water and dried at 100 ºC for 24 h. The solid mass was then carefully ground in a mortar and finally calcined at 700 ºC for 6 h. The cobalt content was fixed such that the finished catalysts contained 1 mol of Co in the mixed oxides.

2.2 Characterization techniques

BET surface areas were determined by N_2 adsorption on a SMART SORB 92/93 instrument (Ms. SMART Instruments, India). Prior to the measurement, the samples were dried at 150 ºC for 2 h. X-ray diffraction (XRD) patterns of the catalysts were obtained on an Ultima-IV diffractometer (M/s. Rigaku Corporation, Japan) using nickel-filtered Cu Kα radiation (λ= 1.54 Å). The nature of the phase in the sample was checked using the data base of the Joint Committee on Powder Diffraction Standards (JCPDS). FT-IR spectra were recorded on a Biorad-Excalibur series (USA) spectrometer using the KBr disc method. Temperature programmed reduction (TPR) of the sample was performed in a flow of 5% H_2/Ar gas mixture flowing at a rate of 30 mL/min with a temperature ramp of 10 °C/min. Prior to the TPR run, the sample (20 mg) was pretreated with Ar at 200 ºC for 2 h. The hydrogen consumption was monitored by using the thermal conductivity detector (TCD) of a gas chromatograph. Scanning electron microscopic pictures of the catalysts were obtained on a S-520 electron microscope (M/s. Hitachi Japan) running at an accelerated voltage of 10 kV. The samples were mounted on aluminum stubs using double-adhesive tape and gold coated in a Hitachi HUS-5GB vacuum evaporator. The Raman spectra of the samples were collected on a Horiba-Jobin Yvon LabRam-HR spectrometer equipped with a confocal microscope, 2400/900 grooves/mm gratings, and a notch filter. The visible laser excitation at 532 nm (visible/green) was used. The scattered photons were directed and focused onto a single-stage monochromator and measured with a UV-sensitive LN_2-cooled CCD detector.). XPS measurements were conducted on a KRATOS AXIS 165 with a dual anode (Mg and Al) apparatus using Mg Kα anode. The non-monochromatized Al Kα X-ray source ($h\upsilon$) 1486.6 eV) was operated at 12.5 kV and 16 mA. Before acquisition of the data, the samples were out-gassed for 3 h at 100 °C under a vacuum of 1.0×10^{-7} torr to minimize surface contamination. The XPS instrument was calibrated using Au as standard. For energy calibration, the carbon 1s photoelectron line was used. The carbon 1s binding energy 285 eV was taken as reference. A charge neutralization of 2 eV was used to balance the charge up of the sample. The spectra were deconvoluted using a Sun Solaris based Vision-2 curve resolver. The location and the full width at half-maximum (FWHM) value for the species were first determined using the spectrum of the pure sample. Symmetric Gaussian shapes were used in all cases. UV-Vis DRS spectra were recorded in the region of 200-800 nm at a split width of 1.5 nm and scan speed of 400 nm/min with GBC Cintra 10e spectrometer. Pellets were made from the solid mixture contaianing 15 mg of the sample and required quantity of dried KBr, ground thoroughly for uniform mixing. The spectra were recorded at room temperature. H_2 Chemisorption studies were performed using an Autosorb iQ (Quantachrome USA) unit. Catalyst samples (100 mg), taken in a quartz reactor, were first reduced in H_2 gas at a flow rate of 60 mL/ min and with a heating rate of 10 $^{\circ}$C/min up to 650 $^{\circ}$C. The samples were then flushed with He for 1 h followed by cooling. H_2 gas was then introduced in pulses and the adsorption uptake was analyzed using the thermal conductivity detector of a gas chromatograph. The coke content of the used catalysts was determined in a CHNS analyzer (ElementaV, Germany). Elemental anaysis was carried out to know the compostion of the mixed oxides using the Atomic Absorption Spectrometer (AAS) (M/s ANALYST-300, PERKIN-ELMAR, USA). BET, XRD, FT-IR, Laser Raman, and UV-DRS characterizations were also carried out on the reduced catalysts to investigate the structural changes during reduction. The catalysts were reduced with H_2 (30 mL/min^{-1})at 650 °C/5h cooled to the room temperature and passivated with N_2 flow, before the analysis.

2.3 Reforming activity

Steam reforming of glycerol was performed in a fixed bed reactor. About 1g of the catalyst was loaded in the middle of the reactor, suspended between two quartz wool plugs. Prior to the reaction, the catalyst was reduced with pure hydrogen (100mL/min) for 5h at 650 $^{\circ}$C. After reduction, the hydrogen gas was swept away with N_2 and the reactor bed temperature was brought to the required level under N_2 flow. An aqueous solution of 30 wt.% glycerol was introduced into the preheater, kept above the reactor, at a rate of 0.08 mL/h using a HPLC pump (LabAlliance). After reaching the steady state, over a period of 1 h, the product mixutre coming out of the reactor was condensed , the liquid products seperated in a gas-liquid seperator and the gas products analyzed, on-line using a gas chromatograph (Agilent,7820A) equipped with a carboseive packed column for quantifying H_2, CO, CH_4 and CO_2. The liquid products (acetone, hydroxy acetone, methanol, ethanol and 1,2- and 1,3-propanediol) and unreacted glycerol were analzed by gas chromatograph using an innowax capilary column. The data acquisition was done using the following equations.

$$H_2\ \text{yield}=\frac{H_2\ \text{Produced experimentally}}{H_2\text{Calculated theoretically}}\times 100\%$$

$$H_2\ \text{selectivity}=\frac{\text{molecules of } H_2 \text{ produced experimentally}}{\text{C atoms in gas products}}\times\frac{1}{R}\times 100\%;$$

R is the H_2/CO_2 reforming ratio (7/3) for glycerol.

$$\text{Carbon conversion to vapour}=\frac{\text{C in the gas products}}{\text{C fed into reactor}}\times 100\%$$

$$i\ \text{selectivity}=\frac{\text{i Produced experimentally}}{\text{C atoms in gas products}}\times 100\%;$$

where i is CO, CH_4 and CO_2 produced experimentally.

3. Results and discussion

3.1 AAS, BET surface area and X-ray diffraction

Table 1. Catalysts composition determined from AAS

Catalysts	La		Ce		Co	
	a	b	a	b	a	b
$La_{0.9}Ce_{0.1}CoO_3$	64.23	0.895	06.94	0.097	28.83	0.955
$La_{0.7}Ce_{0.3}CoO_3$	49.50	0.699	20.78	0.296	29.72	0.998
$La_{0.5}Ce_{0.5}CoO_3$	35.67	0.499	35.22	0.497	29.11	0.968
$La_{0.3}Ce_{0.7}CoO_3$	20.12	0.277	50.10	0.698	29.78	0.978
$La_{0.1}Ce_{0.9}CoO_3$	06.90	0.097	63.27	0.898	29.83	0.998

a= wt .% , b= molar ratio

The composition of the catalysts, determined by the AAS (Table 1) clearly matches with those of thereotical values. In all the catalysts, the AAS results clearly indicate that the variation of La/Ce with fixed Co loading is in accoradnce with the catalyst composition.

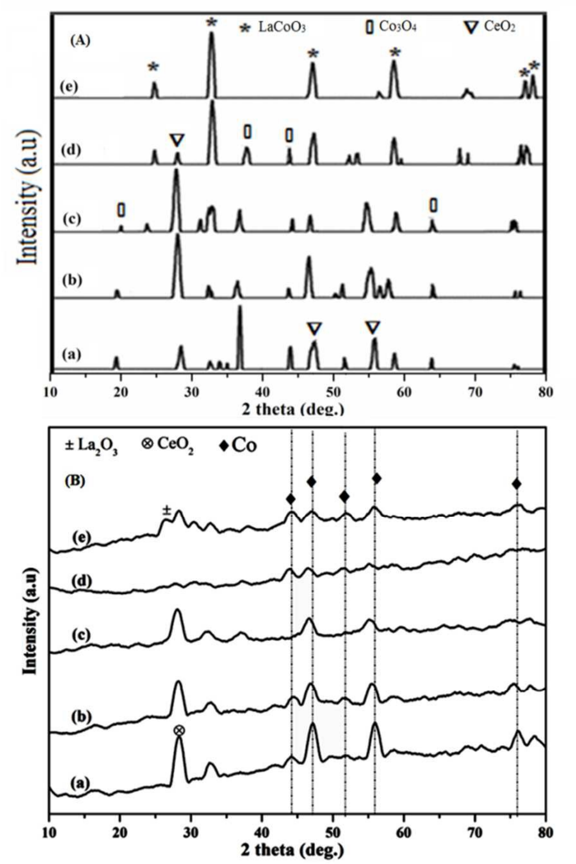

Fig. 1 XRD Patterns of (A) calcined and (B) reduced catalysts
(a) $La_{0.1}Ce_{0.9}CoO_3$ (b) $La_{0.3}Ce_{0.7}CoO_3$ (c) $La_{0.5}Ce_{0.5}Co\ O_3$ (d) $La_{0.7}Ce_{0.3}Co\ O_3$ (e) $La_{0.9}Ce_{0.1}Co\ O_3$

BET area values of the samples are presented in the Table 2.

The surface area of the fresh catalysts dropped from 20.1 to 8.5 m^2/g with increasing La content. However, after reduction in hydrogen, the surface area increased with increasing La content upto catalyst $La_{0.7}Ce_{0.3}CoO_3$ and then on it decreased. The decrease in the case of the fresh catalysts may be due to perovskite formation as reported in the literature[44]. In the case of the reduced samples the increase in surface area can be associated with the collapse of the structure and formation on a well dispersed Co on oxide supports.

The XRD patterns of the calcined catalysts are displayed in Fig.1 (A). The peaks appearing at 36.0, 43.7 and 64.0º are assignable to the cubic Co_3O_4 [PCPDF-801541]. The prominent reflections for sample (a) appearing at 28.5, 33.0, 47.4, 56 and 69.4º are characteristic of CeO_2 in its fluorite structure [PCPDF-710567]. Thus, samples from (a) to (c) contain predominantly Co_3O_4 and CeO_2. In the case of samples (d) and (e), the peaks observed at 2θ values of 32.6, 46.7, 58.3 and 76.9º indicate the presence of the characteristic rhombohedral $LaCoO_3$ perovskite [PCPDF-861665]. The peaks due to Co_3O_4 dominated the patterns of low La containing samples, whereas catalyst (e) contained no Co_3O_4. With increasing CeO_2, the substitution of Ce for La seems to have increased, as reflected by the broadening of the lines.

The XRD patterns of reduced samples are displayed in Fig. 1(B). The peaks positioned at 2θ values of 44.1, 51.6 51.7, 55.9 and 75.6° are assigned to the metallic Co particles[45-48]. The peak observed at 28.5° can be assigned to the CeO_2 phase [PCPDF–710567]. CeO_2 undergoes partial reduction during hydrogen treatment. However, the partially reduced phase either remained amorphous or was reoxidized (when exposed to air during the analysis). This indicates that the perovskite structure is destroyed during the reduction process[47].

3.2 Fourier transform infrared spectroscopy

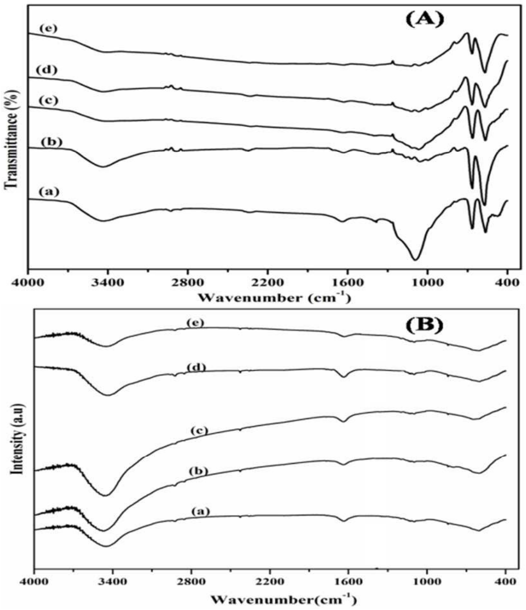

Fig. 2 FT – IR spectra of (A) calcined and (B) reduced catalysts (a) $La_{0.1}Ce_{0.9}CoO_3$ (b)$La_{0.3}Ce_{0.7}CoO_3$ (c) $La_{0.5}Ce_{0.5}CoO_3$ (d)$La_{0.7}Ce_{0.3}CoO_3$ (e) $La_{0.9}Ce_{0.1}CoO_3$

The FT-IR spectra of the calcined mixed oxide samples are shown in Fig. 2(A). The spectra display two distinctive bands originating from the stretching vibrations of the M-O bond. The first band at 570 cm^{-1} is associated with the vibrations in the spinel lattice, where the Co cations exist in an octahedral position and the second band at 661 cm^{-1} is attributed to the $LaCoO_3$ vibrations. The Co/Ce peak intensity ratio decreased with incresing La content, as also reported in the literature[49]. The peak at 3500 cm^{-1} can be attributed to the vibrational frequency of the –OH group of the adsorbed water. The bands at 1038, 1381 and 1633 cm^{-1} correspond to the vibrational frequencies of the residual $\nu(NO_3)^{2-}$ [50,51]. The spectra of the samples show an absorption band at about 1380 cm^{-1} which is the characteristic vibration mode of CeO_2[52]. The fundamental vibrational modes of La-O which normally appear between 920-940 cm^{-1} are not very clear[53]. In the FT-IR spectra of the reduced samples shown in Fig.2(B), the intensity of the bands at 570 and 661 cm^{-1} is considerably decreased indicating the reduction of cobalt oxide to its metallic state.

3.3 Temperature programmed reduction

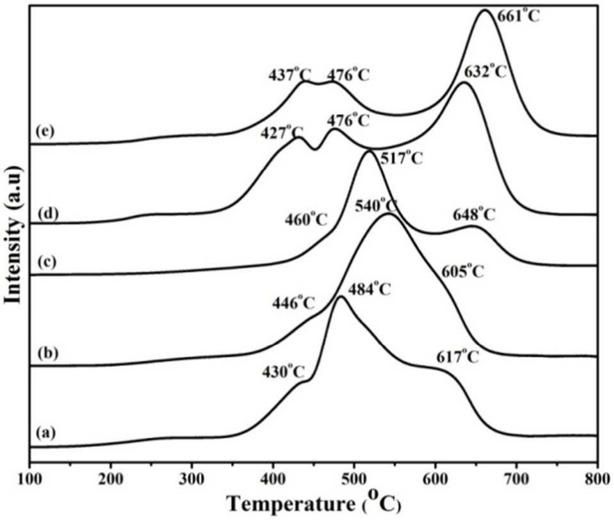

Fig. 3 TPR of (a) $La_{0.1}Ce_{0.9}CoO_3$ (b) $La_{0.3}Ce_{0.7}CoO_3$ (c) $La_{0.5}Ce_{0.5}CoO_3$ (d) $La_{0.7}Ce_{0.3}CoO_3$ (e) $La_{0.9}Ce_{0.1}CoO_3$

The TPR patterns shown in Fig. 3 can be divided into two groups; the high Ce containing ((a) to (c)) and the low Ce containing ((d) and (e)) ones. In the case of catalysts with higher Ce content the reduction peak maxima are seen at lower temperatures due to the presence of well dispersed, small Co_3O_4 particles in intimate contact with CeO_2 and are quite identical with the cerium supported cobalt oxide. The small hump in the beginning of the first peak at 430 °C represents the isolated cobalt oxide species and the reduction peak at 484 °C corresponds to the reduction of Co^{3+} to Co^{2+}, while the second reduction peak at 617 °C represents the reduction of Co^{2+} to Co^0. In the first three catalysts, CeO_2 supports the reducibility of Co_3O_4. With decreasing Ce content this effect decreases. This is reflected in the positions of the peak maxima[54]. The reduction profile of the $LaCoO_3$ perovskite is different from the simple cobalt oxide supported on La_2O_3. In samples (d) and (e) the formation of the perovskite occurs, as shown in the XRD patterns. These TPR profiles are also similar to the ones reported in the literature[55, 56]. The high temperature peak is shifted to higher region. In sample (d) this peak is observed at relatively lower temperature (632 °C) than in sample (e) because of the presence of more amount of Ce in (d).

3.4 Scanning electron microscopy

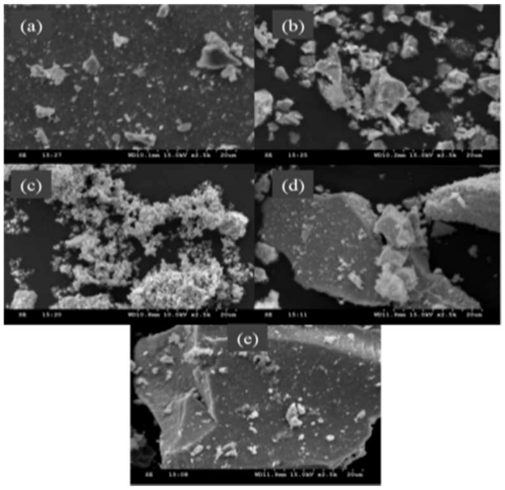

Fig. 4 SEM images of (a) $La_{0.1}Ce_{0.9}CoO_3$ (b) $La_{0.3}Ce_{0.7}CoO_3$ (c) $La_{0.5}Ce_{0.5}CoO_3$ (d) $La_{0.7}Ce_{0.3}CoO_3$ (e) $La_{0.9}Ce_{0.1}CoO_3$

The SEM images of the fresh catalysts are shown in Fig. 4. The particle dimensions seem to have changed with composition. Samples (a) to (c) display fine distribution of mixed oxide particles. The formation and development bulk $LaCoO_3$ particle could be seen in samples (d) and (e). The decrease in BET surface area (Table 1) of fresh samples supports this observation.

3.5 Laser Raman

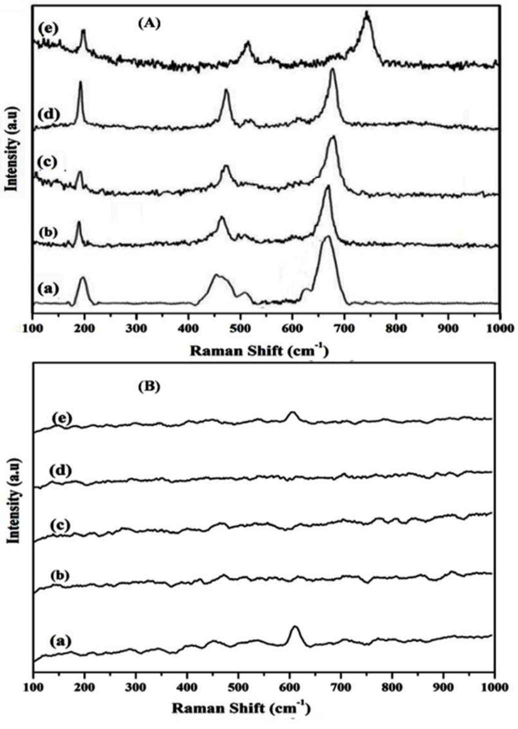

Fig. 5 Laser Raman of (A) calcined and (B) reduced catalysts ; (a) $La_{0.1}Ce_{0.9}CoO_3$ (b) $La_{0.3}Ce_{0.7}CoO_3$ (c) $La_{0.5}Ce_{0.5}CoO_3$(d) $La_{0.7}Ce_{0.3}CoO_3$ (e) $La_{0.9}Ce_{0.1}CoO_3$

The Laser Raman spectra of the calcined and reduced samples are presented in Fig. 5(A) & 5 (B), respectively. The five active modes A_{1g} (679 cm^{-1}), F_{2g} (619, 515 and 192 cm^{-1}) and Eg (473 cm^{-1}) for the cobalt oxide species are observed in all the samples[57-62]. Raman band at high frequency A_{1g} (679 cm^{-1}) can be attributed to the characteristic vibration of oxygen atom inside the CoO_6 octahedral unit[63], whereas F_{2g} and Eg modes are due to the vibration of tetrahedral (CoO_4) and octahedral sites[64]. In sample (d), the width of the peaks is small indicating the formation of the perovskite. The major red shift in the Raman spectrum of catalyst (e) is because of factors like increase in particle size and crystallinity[65]. The larger crystal size is also reflected in TPR, XRD and SEM Results. In the reduced samples the above characteristic peaks are cospicuoulsy absent indicating the formation of metallic Co as a consequence of reduction.

3.6 X-ray photoelectron spectroscopy

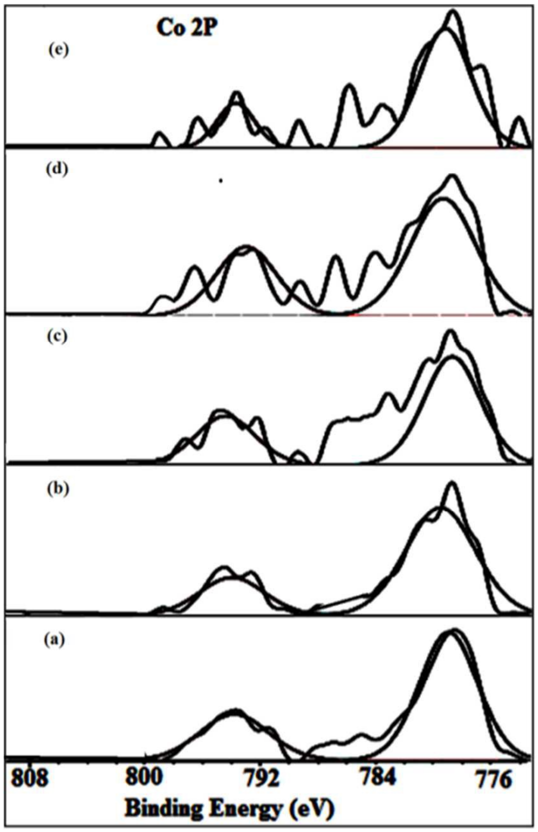

Fig. 6 Co 2p XPS spectra of calcined (a) $La_{0.1}Ce_{0.9}CoO_3$ (b) $La_{0.3}Ce_{0.7}CoO_3$ (c)$La_{0.5}Ce_{0.5}CoO_3$ (d) $La_{0.7}Ce_{0.3}CoO_3$ (e) $La_{0.9}Ce_{0.1}CoO_3$

Co2p XPS spectra: Co2p XPS spectra are shown in Fig. 6. The core level peaks of the $Co2p_{3/2}$ (B.E.:779.2–780.2 eV) and $Co2p_{1/2}$ (B.E.: 794.1–795 eV) observed for the calcined catalysts are quite identical with the B.Es reported for the CoO in equilibrium with Co_3O_4[66]. The intensity of the satelite peaks positioned at ~ 6 eV increased from (a) to (c) indicating that the proportion of the Co_3O_4 is more in these samples. Particularly, in sample (d) the intesity of the 791.1 eV peak increased and has become equal to the intensity of the 787.8 eV peak clearly indicating that cobalt existed as CoO along with Co_3O_4 in $LaCoO_3$ perovskite.

O 1s XPS spectra: The spectra of O1s are presented in Fig.7. Two B.Es are identified for oxygen; the first peak between 529.9-530.2 eV and the second between 531.1-531.9 eV. These peaks can be assigned to the O attached to the Co metal of CoO and the O present in water and surface adsorbed O-H group attached to the Co metal, respectively. From the O 1s XPS spectra it is obsereved that the B.E of the oxygen attached to Co metal increased with increasing the La_2O_3 content. The peak intensity of the lattice oxygen increased with La_2O_3 content in the catalysts [66].

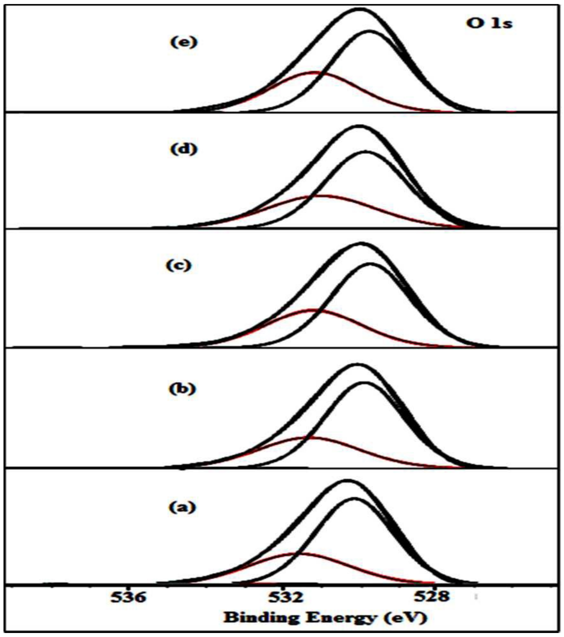

Fig. 7 O 1s XPS spectra of calcined (a) $La_{0.1}Ce_{0.9}CoO_3$ (b) $La_{0.3}Ce_{0.7}CoO_3$ (c) $La_{0.5}Ce_{0.5}CoO_3$ (d) $La_{0.7}Ce_{0.3}CoO_3$ (e) $La_{0.9}Ce_{0.1}CoO_3$

3.7 UV-DRS

The UV-DRS spectra of the calcined and reduced samples are shown in Fig. 8(A) & (B), respectively. UV-DRS is an important technique to know the geometry of the metal centres existing in the material. The band found at 260 nm is purely due to the charge transfer of the oxygen to ligand in the metal oxide. The bands located at 380 and 660 nm resemble that of Co_3O_4 structure. The broad band obtained in the 540-750 nm region is a result of the combination of the Co^{2+} present in the tetrahedral (Td) and the Co^{3+} present in the octahedral position (Oh). The formation of the perovskite structure is evidenced with the blue shift of the 380 and 660 nm bands observed for the samples (d) and (e). This is because of the incorporation of Co in the perovskite geometry [67- 69].

The UV-Vis DRS spectra of the reduced samples do not reveal the characteristic bands of Co^{3+} or Co^{2+} belonging to the octahedral or tetrahedral sites. Only the charge transfer bands of the O → Ce (CeO_2) and O → La (La_2O_3) vibrational bonds are present, as also reported in the literature[70,71]. This information further supports the XRD and FT- IR results of the reduced samples.

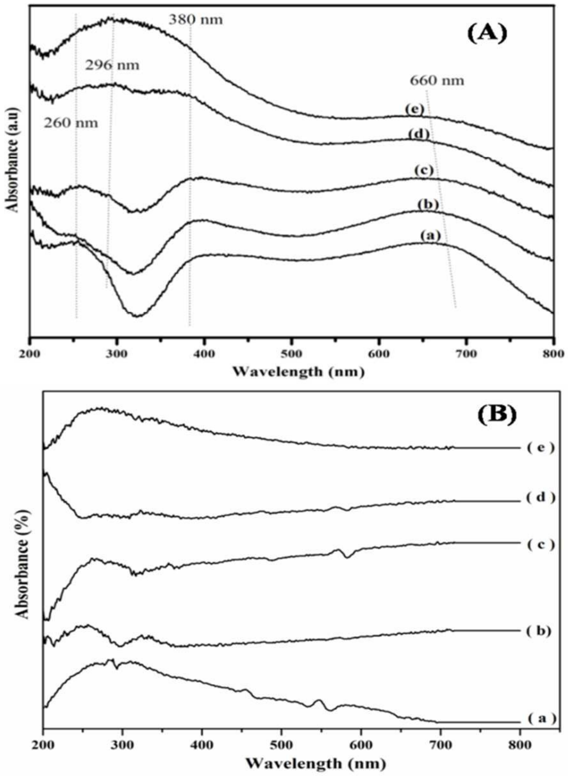

Fig.8 UV- DRS of (A) calcined and (B) reduced catalysts; (a) $La_{0.1}Ce_{0.9}CoO_3$ (b) $La_{0.3}Ce_{0.7}CoO_3$ (c) $La_{0.5}Ce_{0.5}CoO_3$(d) $La_{0.7}Ce_{0.3}CoO_3$ (e) $La_{0.}9Ce0._1CoO_3$

3.8 Catalytic activity

Glycerol steam reforming is a metal-active reaction. Hence, metal dispersion plays a promising role. The values of dispersion of Co, as determined by the H_2 pulse chemisorptions, are presented in Table 1. It can be observed that the active metal dispersion increased with increasing La content and the highest dispersion is achieved for the sample $La_{0.7}Ce_{0.3}CoO_{3.}$ Further increase of La decreased the metal dispersion. This could be due to the formation of the perovskite ($LaCoO_3$) in the fresh sample and also the larger particle size.

All the catalysts showed complete conversion of glycerol, due to high reaction temperature. However, the hydrogen yield varied with temperature, as shown in Fig. 9(A). The hydrogen yield increased with increasing temperature because of the endothermic nature of the reaction.

The progress of steam reforming depends on the reducibility of the metal oxide[72]. Among, all the catalysts studied $La_{0.7}Ce_{0.3}CoO_3$ exhibited the highest hydrogen yield (68%) at 700 °C. This is due the presence of easily reducible Co species with suitable crystal dimensions. When the fresh samples are reduced at higher temperatures, the perovskite structure collapses leading to the formation of well dispersed Co species[73-75], as evidenced by the XRD patterns of the reduced catalysts.

Table 2 BET surface area, H_2 chemisorption and CHNS data

Catalyst	BET surface area Fresh samples (m^2/g)	BET surface area Reduced samples (m^2/g)	Active Metal Surface Area (m^2/g) [a]	Average crystallite size (nm) [b]	Co Dispersion (%) [c]	Carbon Content (wt. %)
$La_{0.1}Ce_{0.9}CoO_3$	20.1	23.8	20.8	9.7	10.3	3.7
$La_{0.3}Ce_{0.7}CoO_3$	16.8	38.0	31.6	6.4	15.6	2.8
$La_{0.5}Ce_{0.5}CoO_3$	12.6	43.4	40.7	5.0	20.1	1.7
$La_{0.7}Ce_{0.3}CoO_3$	11.3	58.0	45.2	4.5	22.2	0.7
$La_{0.9}Ce_{0.1}CoO_3$	8.5	19.0	15.0	13.5	7.4	2.4

a Active metal surface area $(ASA) = (Nm \times S \times Am)/166$ where ASA is in m^2 per gram of sample, b $Average\ particle\ size(d) = \frac{100\times L\times f}{ASA\times Z}$; c $Dispersion\ (D) = \frac{Nm\times S\times M}{100L}$; Nm = The number of adsorbed gas molecules, S = adsorption stoichiometry, Am = The cross-sectional area occupied by each active metal surface atom, M and L are the molecular weight and percent loading of the supported metal, f is a particle shape correction factor (= 6 for spherical particles). Z = density of the supported metal

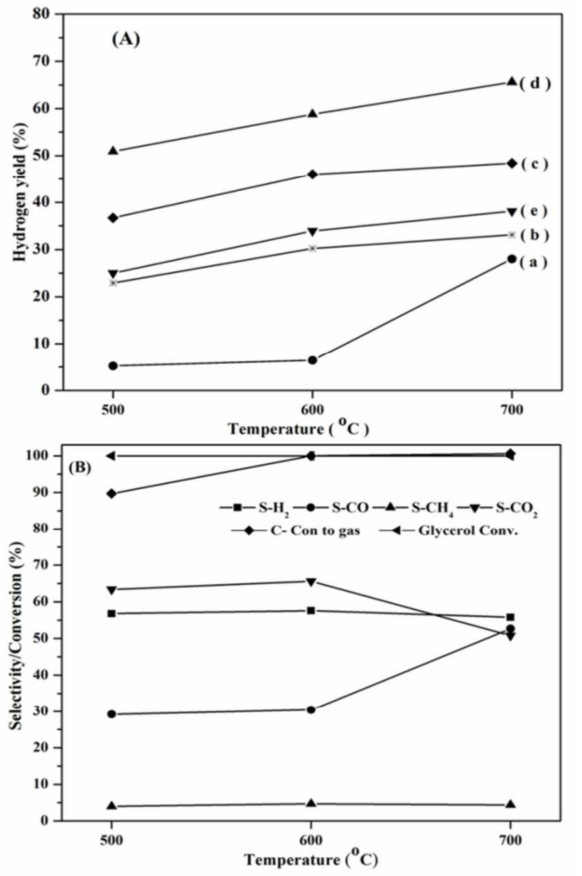

Fig.9.(A) & (B) activity results of ; (a) $La_{0.1}Ce_{0.9}CoO_3$ (b) $La_{0.3}Ce_{0.7}CoO_3$ (c) $La_{0.5}Ce_{0.5}CoO_3$(d) $La_{0.7}Ce_{0.3}CoO_3$ (e) $La_{0.9}Ce0_{.1}CoO_3$

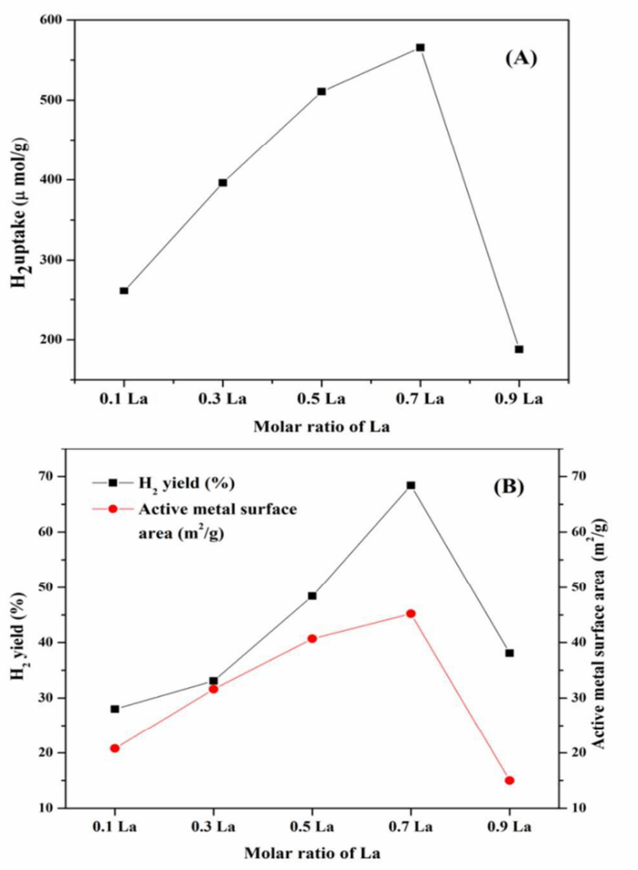

Fig. 10 (A) The variation of H_2 uptake, (B) metal surface area and hydrogen yield with La content

The distribution of gases in the overall reaction products is depicted in Fig. 9(B). The entire carbon in glycerol is converted to carbon products beyond 600 °C, at which the CO_2 formation started decreasing with simultaneous increase in CO composition. The selectivity towards hydrogen almost remained constant. An interesting feature of the catalyst is that the amount of methane formed is very low.

In order to verify the effect of dispersion on the activity, hydrogen chemisorption was carried out on these catalysts. The Co dispersion and particle size are presented in Table 2. It is interesting to observe that the major portion of total surface area of the reduced catalyst (approx. 80%) is due to the contribution of small Co particles. That is the reason why the BET area of the reduced catalysts follows similar trend as that of the fresh catalysts. The H_2 uptake which is used to calculate the active metal area follows similar trend (Fig. 10(A)). Fig. 10(B) shows a nearly parallel behavior existing between the metal surface area and the hydrogen yield, when drawn against the La content in the catalysts. It can be observed from the Table that the dispersion is the highest in the case of $La_{0.7}Ce_{0.3}CoO_3$ catalyst.

Turn over frequency (TOF), is a measure of rate of H_2 production per active cobalt site per second. In the present study

Table 3. Activity comparison with literature reported values

S. No	catalysts	Reaction conditions	Glycerol conversion	Hydrogen	Reference
1	NiO (24.1 %)-MgO (26.1 %) Al_2O_3(49.8%)	650 °C, 1 atm 1.0 g, 10 wt% glycerol	88.0% at 650 °C.	selectivity 78.5 %	77
2	$La_{0.5}Ca_{0.5}NiO_3$	550 °C, 1 atm S/C = 3.0	100% at 550 °C	Yield 82.2%	78
3	Ni 29.2 wt%–Cu31.1 wt%–Al 39.7wt%	600 °C, 1 atm, 1.0g S/C= 3.0	71.9%at 600 °C.	selectivity 78.6%.	79
4	$La_{0.5}Ce_{0.5}NiO_3$	700 °C,1 atm, 1.0g 30 wt.%	88% at 700 °C	selectivity 70 %	80
5	$La_{0.7}Ce_{0.3}CoO_3$	700 °C, 1 atm, 1.0g 30 wt.% glycerol, 0.08 mL min^{-1}	100% at 700 °C	yield 68 %	Present study

H_2-chemisorption technique was used to find out the number of surface cobalt atoms. TOF is found to be sensitive to the particle size. Literature also reports that the activity of carbon nano fibre supported Co catalyst in the FT synthesis depends on the Co particle size and the TOF with respect to hydrogen consumption increases with increase in Co particle size and reaches a maximum when Co particle size is 6 nm[76]. In the present investigation also, a particle size of 4-5 nm seems to be the optimum value for getting high TOF. This behaviour is displayed in Fig. 11, drawn to explain the variation of TOF with Co metal area. The turnover frequency increased steadily with metal surface area (upto 40.7 m^2/g), beyond which a sudden jump is noticed. The rate of hydrogen production reached its maximum (68% yield) as the particle size corresponding to the metal area of 45.2 m^2/g is approached. The highest metal area is achieved for the catalyst $La_{0.7}Ce_{0.3}CoO_3$. Table 2 also discloses the extent of coke formation, analyzed after the reaction. It is also found to be the lowest for this catalyst.

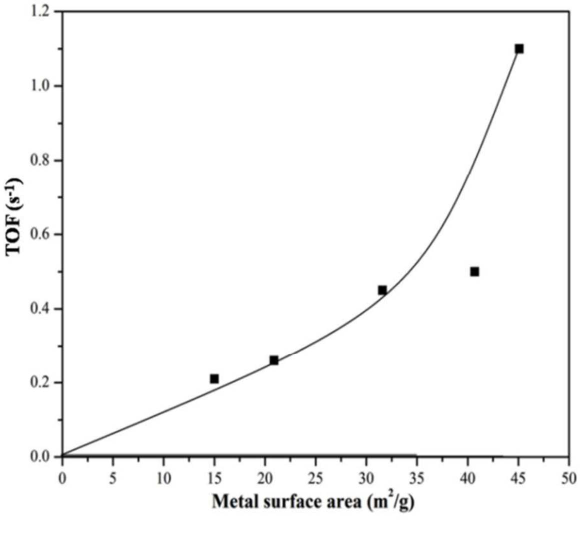

FIg. 11 Variation of TOF with metal surface area

Glycerol conversion and hydrogen yield depend upon the nature of the catalyst, the steam/glycerol (S/C) ratio and reaction temperature. Even though, a direct comparison is not possible, Table 3 displays the recent literature reports on hydrogen generation from glycerol using different catalysts along with the optimum catalyst identified in this work. It can be observed that $La_{0.7}Ce_{0.3}CoO_3$ compares well or even better in some cases.

4. Conclusions

The Co catalysts derived from La-Ce-Co mixed oxides are active for the glycerol steam reforming producing hydrogen-rich gas products. Characterization of reduced catalysts reveals the structure collapse and dispersion of smaller Co metallic particles on the mixed oxide (La_2O_3-CeO_2) support. It is possible to tune the dispersion of Co metal (obtained after reduction of the fresh catalysts), and thus the reforming activity and coke formation by using different Co-containing mixed oxides as starting materials. Lanthana plays a vital role in the enhancement of metal active surface area as well as the dispersion. $La_{0.7}Ce_{0.3}CoO_3$ is found to be the best initial composition for arriving at the maximum hydrogen yield. The active metal area with major share in total area of the reduced samples correlates well with the TOF. It can be concluded that the Co metal dispersion is proportional to hydrogen yield and minimizes coke formation on the catalyst surface.

Acknowledgements

The authors thank Council of scientific industrial research & Department of Science and Technology (DST), New Delhi.

References

1 B. Zhang , X. Tang, Y. Li, Y. Xu, W. Shen, *Int. J. Hydrogen Energy* 2007, **32**, 2367.
2 P.R. d. l. Piscina, N. Homs, *Chem. Soc. Rev.*, 2008, **37,**2459.
3 C.H. Zhou, J.N. Beltramini, Y.X. Fan, G.Q. Lu, *Chem. Soc. Rev.*, 2008, **37,**527
4 J.W. Shabaker, G.W. Huber, J.A. Dumesic, J. Catal. 2004, **222**,180..
5 J. Fermoso, L. He, D. Chen, *Int. J. Hydrogen Energy*, 2012,**37,**14047.
6 R.D. Cortright, R.R. Davda, J.A. Dumesic, *Nature,* 2002, **418,**964.
7 G.W. Huber, J.W. Shabaker, J.A. Dumesic, *Science,* 2003, **300,**2075.
8 R.R. Soares, D.A. Simonetti, J.A. Dumesic, *Angew. Chem. Int. Ed.,* 2006, **45**, 3982.
9 A.O. Menezes, M.T. Rodrigues, A. Zimmaro, L.E.P. Borges, M.A. Fraga, *Renew.Energy,* 2011, **36,** 595.
10 D.A. Simonetti, E.L. Kunkes, J.A. Dumesic, *J. Catal,* 2007, **247,** 298.
11 S. Adhikari, S. Fernando, A. Haryanto, *Energy Fuels,* 2007, **21,**2306.
12 G.R. Moradi, M. Rahmanzadeh,*Catal. Commun.*, 2012,**26**,169.
13 T. Borowieck, *Appl.Catal.*, 1984,**10**,273.
14 S. Adhikari, S. Fernando, A. Haryanto, *Catal. Today*, 2007,**129** 355.
15 B. Zhang, X. Tang, Y. Li, Y. Xu, W. Shen*, Int. J. Hydrogen Energy* 2007,**32,**2367.

16 M. Slinn, K. Kendall, C. Mallon, J. Andrews, *Bioresour. Technol.*, 2008, **99,** 5851.

17 S. Adhikari, S.D. Fernando, A. Haryanto, *Renew. Energy,* 2008, **33,** 1097.

18 A. Iriondo, V. L. Barrio, J.F. Cambra, P.L. Arias, M.B. Güemez, R.M. Navarro, M.C. Sánchez-Sánchez, J.L.G. Fierro, *Top. Catal.*, 2008, **49,** 46.

19 B. Dou, C. Wang, H. Chen, Y. Song and B. Xie, *Int.J. Hydrogen Energy*, 2013, **38,** 11902.

20 C. Wang, B. Dou, H. Chen, Y. Song, Y. Xu, X. Du, L. Zhang, T. Luo and C.Tan, *Int.J. Hydrogen Energy*, 2013, **38**, 3562.

21 B. Dou, Y. Song, C. Wang, H. Chen and Y. Xu, *Renew. Sustainable Energy Rev.*, 2014, **30**, 950.

22 P. Y.Hwa, K.J. Yeon, M.D. Ju, P. N. Cook and K.Y. Chul, Res.Chem.Intermed. 2015 http://link.springer.com/article/10.1007/s11164-015-2020-7

23 G. Wu, C. Zhang, S. Li, Z. Han, T.Wang, X .Ma and J. Gong, Acs Sustain. Chem. Eng., 2013, 1, 1052.

24 U. Ahmed, Irvine, John T. S. Energy Fuels 2013, 58, 187.

25 C.Wang, B.Dou, H. Chen, Y.Song, Y. Xu, X. Du, T. Luo and C.Tan, Chem. Eng.J. 2013, 220, 133.

26 Ji, Wei-rong; Zeng, Yu-long; Tan, Ye-bin; Ying, Hui-juan; Zhang, Ying From Zhejiang Gongye Daxue Xuebao (2013), **41**, 6.

27 Zun-Yu Huang, Cheng-Hua Xu, Chuan-Qi Liu, Hui-Wen Xiao, Jun Chen, Yong-Xiang Zhang, Ya-Cong Lei, Korean J. Chem. Eng., 2013, 30, 587.

28 C. A. Franchini, W. Aranzaez, A. M. D. Farias, G. Pecchi and M. A. Fraga , Appl.Catal.B. 2014, 147, 193.

29 G. Wu, S. Li, C.Zhang, T.Wang and J. Gong, Appl.Catal.B., 2014, 144, 277.

30 V. V. Thyssen, T. A. Maia and E.M. Assaf, Fuel, 2013, 105, 358.

31 S. Kitamura, T. Su-enaga, N. Ikenaga, T. Miyake, T. Suzuki., Catal. Lett. 2011, 141, 895.

32 A. Iriondo, M.B. Güemez, V.L. Barrio, J.F. Cambra, P.L. Arias, M.C. Sánchez-Sánchez and R.M. Navarro, J.L.G. Fierro, Stud. Surf .Sci. Catal., 2010, 175, 449.

33 S. Ramesh, E.H. Yanga, J. S. Junga and D.J. Moon, Int.J.Hydrogen Energ., article in press doi:10.1016/j.ijhydene.2015.02.013

34 Y.Cui, V. Galvita, L. Rihko-Struckmann, H. Lorenz, K. Sundmacher, *Appl. Catal.,B:Environ.,*2009, **90**, 29.

35 M.R. Goldwasser, M.E. Rivas, E. Pietri, M.J. Pe´rez-Zurita, M.L. Cubeiro, L. Gingembre, L. Leclercq, G. Leclercq, *Appl. Catal.*, 2003,**225,** 45.

36 E. Pietri, A. Barrios, O. Gonza´lez, M. Goldwasser, M. Pe´rez-Zurita, M. Cubeiro, J. Goldwasser, L. Leclercq, G. Leclercq, L. Gingembre, *Stud. Surf. Sci. Catal.* 2001,**136,** 381.

37 S.M. de Lima, I.O. da Cruz, G. Jacobs, B.H. Davis, L.V. Mattos, F.B. Noronha, *J.Catal.*, 2008, **257,** 356.

38 P. Biswas, D. Kunzru, *Chem. Eng. J.*, 2008, **136,** 41.

39 D. Srinivas, C.V.V. Satyanarayana, H.S. Potdar, P. Ratnasamy, *Appl. Catal.*, A, 2003,**246,**323.

40 C. Diagne, H. Idriss, A. Kiennemann, *Cat. Commn.*, 2002, **12,** 565.

41 N. Srisiriwata, S. Therdthianwonga, A. Therdthianwong, *Int. J. Hydrogen Energy*, 2009, **34**, 2224.

42 B. Valle, A. Remiro, A.T. Aguayo, J. Bilbao, A.G. Gayubo, *Int. J. Hydrogen Energy,* 2013, **38,** 1307.

43 C. A. Franchinia, W. Aranzaezb, A. M. D. de Fariasa,G. Pecchi, M. A. Fragaa, *Appl. Catal.,B:Environ.,* 2014,**147,** 193.

44 B. Seyfi, M. Baghalhaa, H. Kazemian, *Chem.Eng. J.*, 2009, **148**, 306.

45 P. Jana, V. A. P. OShea, J. M. Coronado and D. P. Serrano, *Appl. Catal. A.,* 2013,**467**,371.

46 V. V. Matveev, D. A. Baranov, G. Y. Yurkov , N. G. Akatiev, I. P. Dotsenko and S. P. Gubin, *Chem. Phys. Lett.*, 2006, **422,** 402.

47 L. Huang, M. Bassir and S. Kaliaguine, Mater.Chem. and Phys., 2007,**101**, 259

48 S. S. Y. Lin, D. H. Kim and S. Y. Ha, *Appl. Catal. A.,* 2009,**355**, 69

49 N. E. Machin, C. Karakaya, A. Celepci, *Energy Fuels*, 2008**, 22**, 2166.

50 Orel. Z, *Internet J. Vib. Spec[www.ijvs.com]* 1999,**3,** 4.

51 A.B.P. Lever, E. Mantovani, B.S. Ramaswamy, *Can. J. Chem.,* 1971,**49,** 1957.

52 B. Yan and H. Zhu, J. Nanoparticle. Res., 2008, 10, 1279.

53 B. Klingenberg and M. A.Vannice, Chem. Mater.1996, 8, 2755.

54 R.N.S.H Magalha˜es, F.S. Toniolo, V. T. Silva, M. Schmal, *Appl. Catal: A*, 2010, **388,** 216.

55 L. Huang, M. Bassir, S. Kaliaguine, *Mater. Chem. Phys.*, 2007, **101,** 259.

56 J.A. Villoria, , M.C. Alvarez-Galvan, S.M. Al-Zahrani, P. Palmisano, S. Specchia, V. Specchia, J.L.G. Fierro, R.M. Navarro, *Applied Catal.B: Environ.*, 2011, **105**, 276.

57 L. Xi, Z. Peng, W. Fan, K. Guo, J. Gu, M. Zhao, J. Meng, Mater. Chem. Phys. 46 (1996) 50

58 N. Orlovskaya, D. Steinmetz, S.Yarmolenko, D. Pai, J. Sankar and J. Goodenough, *Phys. Rev. B.*, 2005,**72**, 014122.

59 A. Ishikawa, J. Nohara and S. Sugai, Phys. Rev. *Lett.,* 2000, **93**, 1193.

60 M. Popa, , J. Frantti and M. Kakihana, *Solid State Ionics*, 2002, **154**, 135.

61 W.W.-Ran, X. D. Peng, S.W.Hui, D. Z. Hui, X. Y.Feng and S.G. Xin, *Chin.Phys.Lett.*, 2005, **22**, 2400.

62 D. P. Kozlenko, N. O. Golosova, Z. Jirák, L. S. Dubrovinsky, B. N. Savenko, M. G. Tucker, Y. Le Godec and V. P. Glazkov, Phys. Rev. B, 2007, **75**, 064422.

63 M.Christy, M. R. Jisha,A. R. Kim, K. S.Nahm,, D. J. Yoo, E. K. Suh, T. S. D. Kumari, T. P. Kumar, A. M. Stephan, *Bull. Korean Chem. Soc.* 2011, **32**, 1204.

64 C.F. Windisch, G.J. Exarhos, K.F. Ferris, M.H. Engelhard, D.C. Stewart, *Thin Solid Films*, 2001, **398**, 45.

65 I. Lopes, N. El Hassan, H. Guerba, G. Wallez, A. Davidson, *Chem. Mater.*, 2006, **18,** 5826.

66 C. C. Li, X. M. Yin, T. H. Wang , H. C. Zeng, *Chem. Mater.*, 2009, **21**, 4984.

67 K. Kaviyarasu, A. Raja, P. A. Devarajan *Spectrochim. Acta, Part A*, 2013, **114**, 586.

68 W. Young Jung, Seong-Soo Hong, *J. Ind. Eng. Chem.*, 2013, **19**, 157.

69 J. Yan, M. C. Kung, W. M. H. Sachtler, H. H. Kung, *J. Catal.*, 1997, **172,** 178.

70 M. Guo, J. Lu, Y. Wu, Y. Wang and M. Luo, Langmuir, 2011, **27**, 3872.

71 S. Satish, D.K. Pradhan , G. Hota and B.G. Mishra, Chem. Eng. J., 2012, **193**, 1.

72 L.P.R. Profeti, E.A. Ticianelli and E.M. Assaf, *Int. J. Hydrogen Energy*, 2009, 34, 5049–5060

73 G. Valderrama, M.R. Goldwasser, C.U. d. Navarro, J.M. Tatibouët, J. Barrault, C.Batiot-Dupeyrat, F. Martínez, Catalysis Today 107–108 (2005) 785–791.

74 G.S. Gallego, F. Mondragón, J. Barrault, J.-M. Tatibouët, C. Batiot-Dupeyrat,Applied Catalysis A: General 311 (2006) 164–171.

75 R.M. Navarro, M.C. Alvarez-Galvan, J.A. Villoria, I.D. González-Jiménez, F. Rosa,J.L.G. Fierro, Applied Catalysis B: Environmental 73 (2007) 247–258

76 G. L. Bezemer, J. H. Bitter, H. P. C. E. Kuipers, H. Oosterbeek, J. E. Holewijn, X. Xu, F. Kapteijn, A. J. V. Dillen, K. P. de Jong, *J. Am Chem. Soc.*,2006, **128**, 3956.

77 Chao Wang, Binlin Dou, Haisheng Chen, Yongchen Song, Yujie Xu, Xu Du, Tingting Luo, Chunqing Tan *Chem.Eng.J.*, 2013,**220**, 133.

78 Gaowei Wua, Shuirong Lia, Chengxi Zhanga, Tuo Wanga, Jinlong Gong, *Appl. Catal. B: Environ.*,2014, **144,** 277.

79 Binlin Dou, Chao Wang, Yongchen Song, Haisheng Chen, Yujie Xu, *Energy Conversion and Management ,* 2014,**78,** 253.

80 C. A. Franchini, W. Aranzaez, A. M. D. de Fariasa,G. Pecchi, , M. A. Fraga, *Appl. Catal. B: Environ.,*2014,**147**, 193.

Glycerol steam reforming over La-Ce-Co mixed oxide-derived cobalt catalysts

M. Surendar, T. V. Sagar, B. Hari Babu, N. Lingaiah, K. S. Rama Rao and P. S. Sai Prasad*
Inorganic and Physical Chemistry Division, CSIR – Indian Institute of Chemical Technology,
Uppal Road, Hyderabad – 500 607, India.

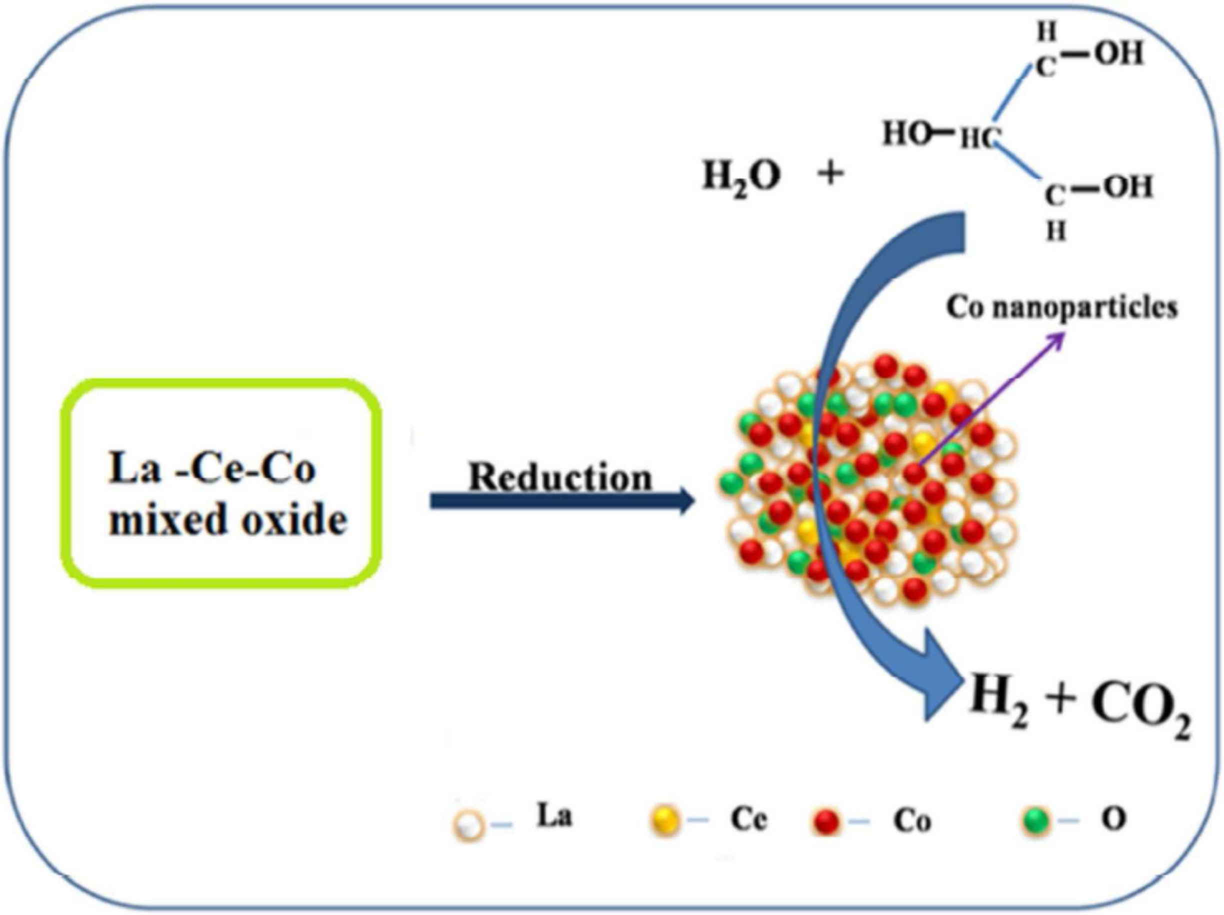

Cobalt nano particles derived from the La-Ce-Co mixed oxide, after reduction, are highly active for the glycerol steam reforming to produce hydrogen.